

Optimizing omnigenity like quasisymmetry for stellarators

Hengqian Liu,* Guodong Yu,* Caoxiang Zhu,† and Ge Zhuang

School of Nuclear Science and Technology and CAS Key Laboratory of Frontier Physics in Controlled Nuclear Fusion, University of Science and Technology of China, Hefei, Anhui 230026, China

(Dated: February 14, 2025)

Omnigenous magnetic fields, where the bounce-averaged radial drift vanishes, offer a promising solution to confine charged particles in fusion devices, particularly in stellarators. However, non-quasisymmetric omnigenity has remained underexplored due to the absence of a general optimization method. We introduce a novel approach for optimizing omnigenity. With simplicity comparable to quasisymmetry (QS) optimization, the new method unifies both QS and non-QS omnigenity optimization and can be further generalized to optimize configurations beyond omnigenity. This approach has led to the realization of precisely omnigenous configurations with exceptional confinement and unprecedented compactness. Additionally, novel configurations like pseudosymmetry and piecewise omnigenity have been directly optimized for the first time. These advances enable efficient explorations of practical stellarator designs with enhanced confinement and engineering feasibility.

Introduction—Stellarators confine plasmas for nuclear fusion using three-dimensional magnetic fields mainly produced by external coils. Without large plasma currents, stellarators can be operated at steady state and are less prone to current-driven instabilities such as disruptions. They have achieved high fusion triple products [1], and recent experiments indicate comparable energy confinement scaling with tokamaks [2]. These advantages establish the stellarator as a promising route to fusion energy.

In toroidal systems, trapped particles bouncing between mirror points typically experience non-zero net radial drifts. This challenge, which historically limited stellarator confinement, can be addressed by imposing specific magnetic field properties.

A widely-used condition, *omnigenity* [3], ensures that the bounce-averaged radial drift vanishes, $\langle \mathbf{v}_d \cdot \nabla \psi \rangle = 0$ (\mathbf{v}_d is the drift velocity and ψ is the flux surface label). Wendelstein 7-X (W7-X), the world’s largest stellarator, employs an omnigenous configuration that significantly reduces neoclassical transport [4] and holds the record stellarator triple product [5]. Omnigenity is closely linked to the second adiabatic invariant, $\mathcal{J} = \int_1^{l_2} mv_{\parallel} dl$ (l is the distance along the field line). The radial drift of trapped particles is $\Delta\psi = q^{-1} \partial\mathcal{J}/\partial\alpha$ (q is the particle charge) [6], where α is the field line label (from the Clebsch form, $\mathbf{B} = \nabla\psi \times \nabla\alpha$). Omnigenous fields have $\partial\mathcal{J}/\partial\alpha = 0$ implying that \mathcal{J} is constant on a flux surface (for particles with the same energy and magnetic moment). The conditions for omnigenity [7] can also be summarized as 1) B_{\min} and B_{\max} having the same value on the flux surface, 2) straight contours for B_{\max} in Boozer coordinates [8], and 3) uniform bounce distance along field lines.

There is a subset of omnigenity called *quasisymmetry* (QS) [9]. The magnetic field strength of QS configurations depends on a single angle in Boozer coordinates, *i.e.*, $B = B(\psi, M\theta - N\zeta)$. The symmetry in B conserves the canonical angular momentum of particles. QS optimization is relatively simple and robust. A standard

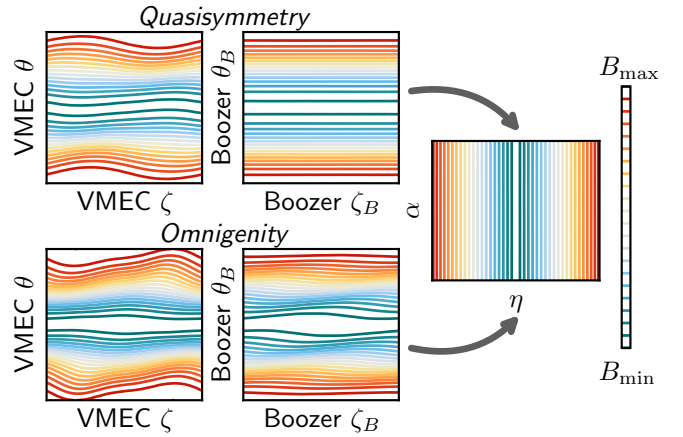


FIG. 1: Magnetic field strength contours in different coordinates for quasi-axisymmetry (top row) and toroidal omnigenity (bottom row).

way is to reduce the asymmetric components in Boozer coordinates. The simplicity of QS optimization has led to great success. The first fully optimized stellarator design is a quasi-helically symmetric configuration [10], and subsequent advances have produced numerous QS configurations [11–14]. Recent studies demonstrate that QS can be achieved with high precision globally, offering exceptional confinement [15].

Despite being less restrictive than QS, non-QS omnigenity is underexplored. The difficulty arises from the absence of simple optimization methods similar to QS. As shown in Fig. 1, B contours in omnigenous fields are *not* straight in either equilibrium code (VMEC [16]) coordinates or Boozer coordinates. Early omnigenous designs minimized particle losses directly [17], while later approaches optimized the alignment of \mathcal{J} contours with flux surfaces, yielding designs such as QPS [18] and QIPC [19]. Recent works have attempted to minimize the deviation of the equilibrium field from a prescribed omnigenous field [20, 21] or the equilibrium \mathcal{J} from an ideal

\mathcal{J} [22, 23]. Omnigenous configurations have also been derived using near-axis expansions [24–27]. Optimizing fast-ion confinement proxies has led to designs like CIEMAT-Q14 [28, 29].

In this Letter, we propose a novel approach for omnigenity optimization similar to the standard Boozer-coordinates-based QS optimization. After identifying a coordinate system where B -contours are straight along some angle (as shown in Fig. 1), omnigenity can be achieved by reducing asymmetric components. This approach avoids computationally intensive evaluations of \mathcal{J} and does not require pointwise matching in the B -distribution. Due to the analogy with QS optimization, we have optimized a large class of new non-QS omnigenous configurations with exceptional confinement and unprecedented compactness. The new approach unifies both QS and non-QS omnigenity optimization and can be further generalized to obtain optimized configurations beyond omnigenity.

Methods—The new method adopts a coordinate transformation similar to the Cary-Shasharina (C-S) one [7, 30]. The C-S coordinate transformation and its generalizations [21, 31] provide a way to construct an exact omnigenous field with a mapping \mathcal{M} from the (α, η) coordinates to the Boozer coordinates (θ_B, ζ_B) . Since constant η contours represent B contours *a priori*, the strength of the constructed omnigenous field in the (α, η) coordinates depends only on η . For a different equilibrium away from omnigenity, the B distribution in the original (α, η) coordinates can be obtained by using the inverse mapping \mathcal{M}^{-1} and will *not* be straight anymore. In analogy to QS, the (α, η) coordinates can be used as the general basis and reducing the symmetry-breaking modes will lead to omnigenity. Instead of matching the B distribution pointwisely, the new method imposes fewer constraints by only optimizing $\partial B / \partial \alpha = 0$ and thus can explore more solutions.

We employ a modified C-S coordinate transformation. An intermediate coordinate system $(\tilde{\theta}, \tilde{\zeta})$ is used to construct the transformation from (α, η) to (θ_B, ζ_B) . We choose $\tilde{\theta} = \alpha$ and define $\tilde{\zeta}$ as

$$\tilde{\zeta}(\alpha, \eta) = \eta - D(\eta) \cdot S(\alpha, \eta), \quad (1)$$

where $\alpha \in [0, 2\pi)$ labels field lines and $\eta \in [-\pi, \pi)$ labels B contours ($\eta = 0$ for minimum B and $\eta = \pm\pi$ for maximum B). Here, $S(\alpha, \eta)$ controls the contour shape and $D(\eta)$ determines the bounce distance between two equal magnetic field contours along field lines. To preserve stellarator symmetry, $S(\alpha, \eta)$ is chosen to be an odd function and $D(\eta)$ is an even function, expressed using Fourier series as

$$\begin{cases} S(\alpha, \eta) = \sum_m s_m \sin[m\eta(\alpha, \eta)], \\ D(\eta) = \sum_n d_n \cos\left[\left(n + \frac{1}{2}\right)\eta\right], \end{cases} \quad (2)$$

where s_m and d_n are Fourier coefficients.

Field strength contours in omnigenous fields can close toroidally, poloidally, or helically, corresponding to *toroidal omnigenity* (TO), *poloidal omnigenity* (PO), and *helical omnigenity* (HO), respectively. The variable $y(\alpha, \eta) = Y[\alpha \ \eta]^T$ is used to control the helicity direction. We choose $Y = [n_{\text{fp}} \ -n_{\text{fp}}/\iota]$ for TO, $Y = [1 \ -\iota/n_{\text{fp}}]$ for PO, and $Y = [1 \ \iota/(\iota + n_{\text{fp}})]$ for HO, where ι is the rotational transform and n_{fp} is the number of field periodicity. The actual Boozer coordinates with field periodicity is then derived with

$$[\theta_B \ \zeta_B]^T = M[\tilde{\theta} \ \tilde{\zeta}]^T, \quad (3)$$

with the matrix M given by

$$\begin{bmatrix} 0 & 1 \\ 1 & 0 \end{bmatrix}, \begin{bmatrix} 1 & 0 \\ 0 & \frac{1}{n_{\text{fp}}} \end{bmatrix}, \begin{bmatrix} 1 & 0 \\ -\frac{1}{n_{\text{fp}}} & -\frac{1}{n_{\text{fp}}} \end{bmatrix},$$

for TO, PO, and HO, respectively. Note that n_{fp} is divided in PO and HO, not TO. This avoids TO having a rotational transform comparable to n_{fp} , which becomes impractical for configurations with large n_{fp} .

Once the coordinate mapping from (α, η) to (θ_B, ζ_B) has been established, omnigenity can be optimized by minimizing asymmetric components,

$$f_{\text{omni}} = \sum_{m \neq 0} (B_{m,n}/B_{0,0})^2, \quad (4)$$

where $B(\alpha, \eta) = \sum B_{m,n} \cos(m\alpha - n\eta)$ and $B_{m,n}$ is computed with Fourier decomposition. This is similar to the standard QS cost function. In particular, QS will be optimized if $S = 0$ is assumed in Eq. 1 which implies straight B contours in Boozer coordinates. f_{omni} can be used in any stellarator optimization codes, *e.g.* STELLOPT [32], SIMSOPT [33], or DESC [34]. The mapping function controlled by S and D is not fixed and could be varied for better numerical convergence. Manipulating the mapping function could allow us to obtain new configurations beyond omnigenity, which will be discussed later.

Precisely omnigenous configurations—Numerical examples of precisely omnigenous configurations with exceptional confinement and low aspect ratios have been obtained. The omnigenity cost function, f_{omni} , has been implemented in the SIMSOPT optimization framework [33]. To obtain practical solutions, additional terms are added to the overall cost function. Here, we have added two more objective functions. The first one is an aspect ratio constraint, $f_{\text{ap}} = (A - A_*)^2$, where A is the flux surface aspect ratio and A_* is the target value. Lower aspect ratios are generally favorable. The second one is a rotational transform constraint, $f_{\bar{\iota}} = (\bar{\iota} - \bar{\iota}_*)^2$, where $\bar{\iota}$ is the rotational transform on the flux surface and $\bar{\iota}_*$ is the target value. The overall objective function is expressed as $f_{\text{total}} = f_{\text{omni}} + w_{\text{ap}} f_{\text{ap}} + w_{\bar{\iota}} f_{\bar{\iota}}$ with w_{ap} and $w_{\bar{\iota}}$ being user-specified weights. Optimization is performed

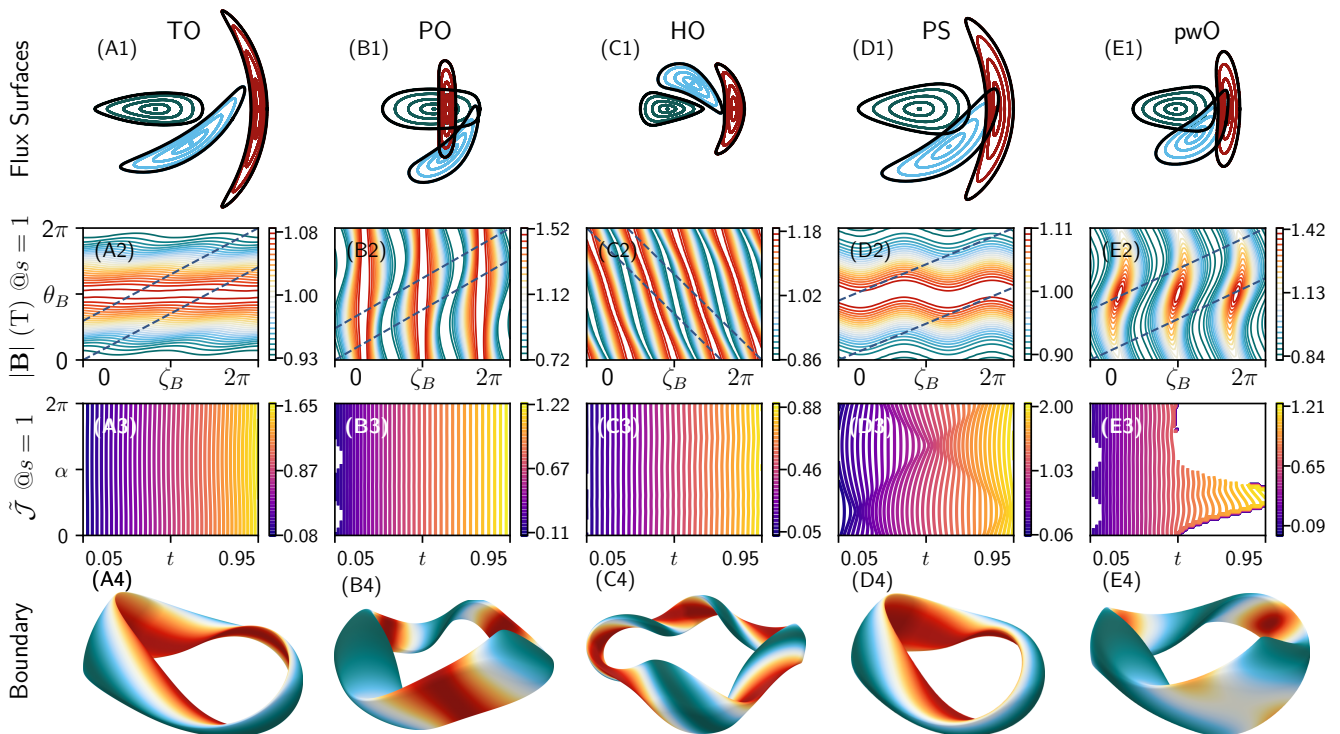


FIG. 2: Gallery of optimized configurations. Column A: toroidal omnigenity (TO), Column B: poloidal omnigenity (PO), Column C: helical omnigenity (HO), Column D: piecewise omnigenity (pwO), and Column E: pseudosymmetry (PS). The first row shows cross-sections of the outermost magnetic surface (LCFS) from VMEC (black solid lines) alongside Poincaré plots from SPEC (colored dots). The second row displays the field strength $|\mathbf{B}|$ on the LCFS in Boozer coordinates. Dashed lines indicate field lines. The third row presents the normalized second adiabatic invariant $\tilde{\mathcal{J}}$ as a function of the relative field strength $t = (B^* - B_{\min}) / (B_{\max} - B_{\min})$. The fourth row illustrates the 3D plasma boundary shape, with colors indicating the field strength as in the second row.

using the trust region reflective optimization algorithm [35] with the plasma boundary shape (*i.e.*, the Fourier coefficients $\{R_{m,n}, Z_{m,n}\}$ in the VMEC equilibrium code [16]) as degrees of freedom.

For demonstration, we have selected three precisely omnigenous configurations with different helicities. The optimization does not need a “warm” start and the initial guess is a circular torus. For TO and HO optimization, better omnigenity is achieved if QA and QH are obtained first. For brevity, the three configurations are vacuum ($\beta = 0$) and omnigenity on the outermost magnetic surface ($s = 1.0$) is optimized. Fig. 2 shows the results, with all configurations scaled to a volume-averaged field strength of 1 T and a major radius of 1 m. For TO (Fig. 2 column A), we set $n_{\text{fp}} = 2$, $A_* = 6$, and $\iota_*^{\text{axis}} = \iota_*^{\text{edge}} = 0.7$. The achieved ι profile is almost constant at $\iota = 0.7$. PO (Fig. 2 column B) has $n_{\text{fp}} = 3$, $A_* = 6.5$, and $\iota_*^{\text{edge}} = 0.76$. The achieved ι ranges from 0.872 on the magnetic axis to 0.76 at the edge. HO (Fig. 2 column C) is optimized with $n_{\text{fp}} = 4$ and $A_* = 8$. The average ι is constrained to be 1.15 in the first stage targeting a QH. The achieved ι ranges from 1.186 to 1.3.

The optimized configurations are verified to have continuous nested magnetic surfaces throughout the volume using the SPEC code [36]. (Detailed Poincaré plots and rotational transform profiles can be seen in the Supplemental Material [37].)

All three configurations demonstrate precise omnigenity. The normalized second adiabatic invariant, $\tilde{\mathcal{J}}(\psi, B^*) = \int_{l_1}^{l_2} \sqrt{B^* - B} dl$, is almost straight along α (Fig. 2 (A3)~(C3)), indicating that $\partial\tilde{\mathcal{J}}/\partial\alpha = 0$ is achieved with high accuracy. The deviation from omnigenity can be quantitatively assessed with the average $\tilde{\mathcal{J}}^{-1}\partial\tilde{\mathcal{J}}/\partial\alpha$, as shown in Fig. 3. These results are compared to the high-mirror configuration of W7-X [38] (W7X-HM), which has the best omnigenity among the W7-X equilibria, and the precise QA case from Landreman & Paul [15] (LP-QA), which has exceptionally high precision in QS. LP-QA can also be reproduced using the new method with the QS optimization capability. The omnigenity residues of TO, PO, and HO are two orders lower than W7X-HM and comparable to LP-QA.

High accuracy in omnigenity leads to exceptional confinement in both collisional transport and collisionless

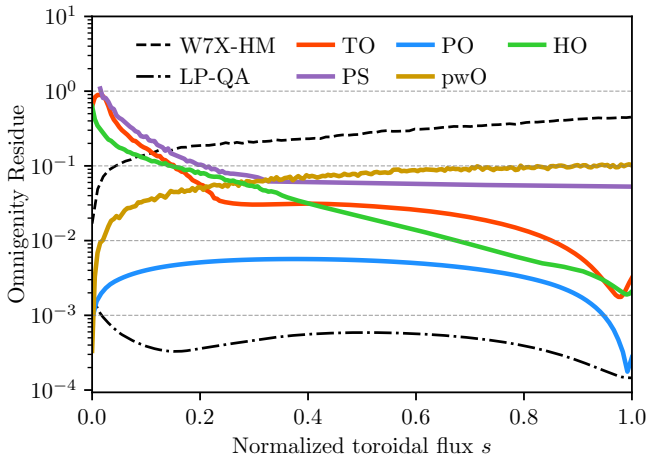


FIG. 3: Radial profiles of the average $\tilde{J}^{-1}\partial\tilde{J}/\partial\alpha$ for measuring the omnigenity residue.

alpha particle losses. As shown in Fig. 4 (a), neoclassical transport in the $1/\nu$ regime (ν is the collisionality), measured by the effective ripple $\epsilon_{\text{eff}}^{3/2}$ calculated using the NEO code [39], is low and certainly smaller than the turbulence transport. Alpha particle confinement is evaluated using the SIMPLE code [40] with settings consistent with Ref. [15]. The configurations are scaled to the ARIES-CS reactor size (minor radius of 1.7 m, average field strength of 5.7 T), and 5000 alpha particles (3.5 MeV, isotropic, initialized at $s = 0.25$) are followed for 0.2 seconds without collisions. The loss fractions of alpha particles in TO and HO are 0.50% and 0.16%, respectively, while PO has no losses before the slowing-down time, as shown in Fig. 4 (b). The obtained configurations demonstrate superior confinement performance compared to any built stellarator, achieving the best performance among the proposed designs (comparable to precise QS). In particular, the aspect ratios are lower than any existing omnigenous configuration (TO: 6.0 vs 19.6 [21], PO: 6.5 vs 8.0 [20], HO: 8.0 vs 18.3 [21]), which will substantially reduce the construction cost.

Configurations beyond omnigenity—Omnigenity is often considered as the minimum requirement for confining all particles. However, several concepts extending beyond omnigenity leverage more general features of the \tilde{J} distribution, including pseudosymmetry [41], bumpy symmetry [42], isometry [43], isodrastic fields [44], and piecewise omnigenity [45]. While not fully eliminating radial drift, these concepts may offer greater design flexibility for future fusion reactors. Our omnigenity optimization method is flexible enough to directly target these conceptual configurations. Here, we focus on pseudosymmetry (PS) and piecewise omnigenity (pwO).

A PS configuration has no locally trapped particles, *i.e.*, the field strength has no locally closed contours. The B -contours cannot be tangent to the magnetic field line

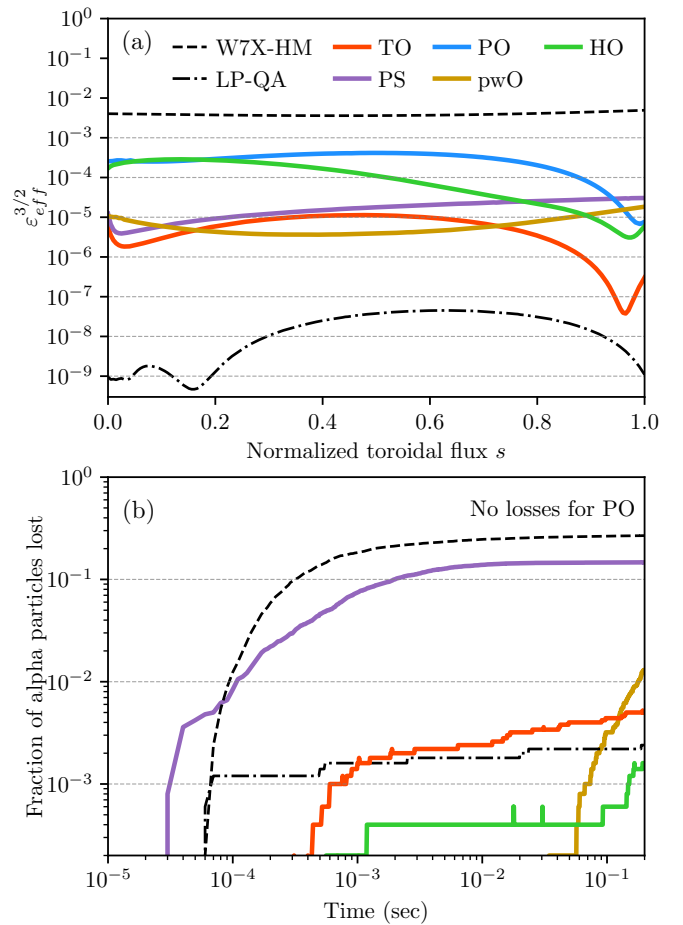


FIG. 4: Confinement of all configurations. (a) Neoclassical transport coefficient $\epsilon_{\text{eff}}^{3/2}$. (b) Collisionless loss fractions of alpha particles at the ARIES-CS reactor size (PO has no losses).

in PS configurations. To achieve PS, the mapping function from (α, η) to (θ_B, ζ_B) is decoupled from the rotational transform ι . A *fictitious* ι is selected for the mapping function and remains constant, while an additional target function enforces non-tangency between B -contours and magnetic field lines. Fig. 2 column D shows a PS configuration with $n_{\text{fp}} = 2$, $A = 5$, and a constant $\iota = 0.39$. The B -contours close toroidally, resembling TO, but the non-tangency condition ensures no neighboring B -lines intersect a field line twice. The field strength along a field line, shown in Fig. 5, confirms the absence of local wells, consistent with Ref. [41]. With the elimination of locally trapped particles, PS has a considerably low $\epsilon_{\text{eff}}^{3/2}$, comparable to TO, as shown in Fig. 4 (a). More interestingly, PS is less elongated than an equivalent TO implying potentially simpler coils and it has a lower aspect ratio which is generally favorable for compact reactors. However, as $\partial\tilde{J}/\partial\alpha = 0$ is not enforced (Fig. 3), PS configurations show non-straight \tilde{J} contours (Fig. 2 (D3)). Consequently, the average radial drift is

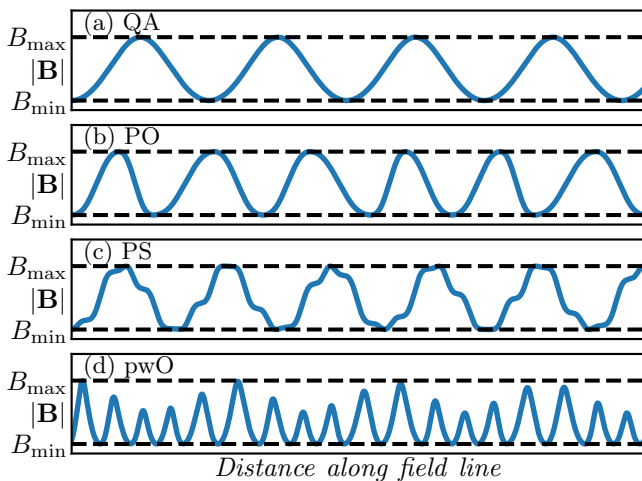


FIG. 5: Field strength distributions along the field line in multiple configurations.

not zero. Fig. 4 (b) confirms that PS has poor alpha-particle confinement with all trapped particles lost.

The pwO concept arises from $\partial\mathcal{J}/\partial\alpha = 0$ being fulfilled piecewisely [45], explaining good confinement in configurations deviating from exact omnigenity. However, there has yet to be a direct optimization method. Our omnigenity optimization method can be adapted to produce pwO configurations by modifying the mapping range of η . In Eq. 1, $\eta \in [-\pi, \pi)$ is used to construct omnigenous fields. For pwO, we can limit the range of η (e.g. $\eta \in [-\pi/2, \pi/2)$) so that neighboring B_{\max} contours intersect with each other. Although the B_{\min} regions are still omnigenous, the “squeezed” B_{\max} regions will form locally closed “islands”. Fig. 2 column E illustrates a pwO configuration resembling PO, with $n_{\text{fp}} = 3$, $A = 6$, $\iota_{\text{edge}} = 0.62$. This pwO optimization starts from a PO with $A = 8$. $\tilde{\mathcal{J}}$ is almost straight in the low-field region, but deviates in the high-field region. The blank areas in the $\tilde{\mathcal{J}}$ plot (Fig. 2 (E3)) correspond to failures in finding paired bounce points in one period due to local ripples. The obtained configuration combines omnigenity (in the low-field region) and pwO (in the high-field region) [46]. Although pwO has a relatively high omnigenity residue (Fig. 3), it shows low $\epsilon_{\text{eff}}^{3/2}$ and alpha-particle loss fractions near 1% at reactor scale. Field strength distributions reveal locally closed contours (Fig. 2 (E2)) and multiple local wells along the field line (Fig. 5), which are different from omnigenity and PS. The minima of B are equally spaced and at the same value, similar to the concept reported by Mynick *et al.* [47]. Almost all trapped particles are well confined in pwO. It is also noted that pwO is less elongated than PO and has a smaller aspect ratio, possibly due to weaker constraints in the B_{\max} region.

Discussions—We have introduced a novel method for optimizing omnigenity by reducing symmetry-breaking

modes in the (α, η) coordinates, which is conceptually as simple as the QS optimization. Besides QS configurations, precisely omnigenous configurations away from QS have been obtained using the new method. These configurations exhibit exceptional confinement in both neoclassical transport and collisionless alpha particles. Notably, TO and HO have significantly lower aspect ratios than previously reported configurations, making them promising candidates for future stellarators. The new method has demonstrated great robustness, with successful optimization starting from a circular torus (“cold” start), and flexibility, enabling the direct optimization of new conceptual configurations beyond omnigenity with minor modifications. For the first time, PS and pwO configurations have been directly optimized. PS and pwO exhibit low neoclassical transport and reduced elongation, potentially simplifying coil designs. These configurations highlight the additional flexibility offered by relaxing the stricter conditions of omnigenity.

While only vacuum configurations are considered here, finite-beta equilibria can be easily obtained using the same method. The omnigenity cost function can be applied to multiple flux surfaces achieving global omnigenity. It can also be combined with other metrics to accommodate additional requirements, such as MHD stability and turbulence transport. Furthermore, engineeringly-feasible coils can be designed using existing tools [48]. The new method opens avenues for deeper exploration within the omnigenity design space. As generalized forms of QA and QH, TO and HO may offer additional degrees of freedom to enhance engineering feasibility. With weaker constraints, PS and pwO demonstrate good confinement while potentially reducing coil complexity. pwO is particularly promising, exhibiting exceptional alpha particle confinement and warranting further investigation.

Acknowledgments—This work was supported by the Strategic Priority Research Program of the Chinese Academy of Sciences under Grant No. XDB0790302 and the Anhui Provincial Key Research and Development Project under Grant No. 2023a05020008.

* These authors contributed equally to this work.

† caoxiangzhu@ustc.edu.cn

- [1] S. E. Wurzel and S. C. Hsu, Progress toward fusion energy breakeven and gain as measured against the Lawson criterion, *Physics of Plasmas* **29**, 062103 (2022).
- [2] U. Stroth, G. Fuchert, M. N. A. Beurskens, G. Birkenmeier, P. A. Schneider, E. R. Scott, K. J. Brunner, F. Günzkofer, P. Hacker, O. Kardaun, J. P. Knauer, K. Rahbarnia, D. Zhang, and M. team, Stellarator-tokamak energy confinement comparison based on ASDEX Upgrade and Wendelstein 7-X hydrogen plasmas, *Nuclear Fusion* **61**, 016003 (2020).
- [3] L. S. Hall and B. McNamara, Three-dimensional equi-

- librium of the anisotropic, finite-pressure guiding-center plasma: Theory of the magnetic plasma, *The Physics of Fluids* **18**, 552 (1975).
- [4] C. D. Beidler, H. M. Smith, A. Alonso, T. Andreeva, J. Baldzuhn, M. N. A. Beurskens, M. Borchardt, S. A. Bozhentkov, K. J. Brunner, H. Damm, M. Drevlak, O. P. Ford, G. Fuchert, J. Geiger, P. Helander, U. Hergenhanh, M. Hirsch, U. Höfel, Y. O. Kazakov, R. Kleiber, M. Krychowiak, S. Kwak, A. Langenberg, H. P. Laqua, U. Neuner, N. A. Pablant, E. Pasch, A. Pavone, T. S. Pedersen, K. Rahbarnia, J. Schilling, E. R. Scott, T. Stange, J. Svensson, H. Thomsen, Y. Turkin, F. Warmer, R. C. Wolf, and D. Zhang, Demonstration of reduced neoclassical energy transport in Wendelstein 7-X, *Nature* **596**, 221 (2021).
- [5] T. Klinger, T. Andreeva, S. Bozhentkov, and W7-X Team, Overview of first Wendelstein 7-X high-performance operation, *Nuclear Fusion* **59**, 112004 (2019).
- [6] P. Helander, Theory of plasma confinement in non-axisymmetric magnetic fields, *Reports on Progress in Physics* **77**, 087001 (2014).
- [7] J. R. Cary and S. G. Shasharina, Helical Plasma Confinement Devices with Good Confinement Properties, *Physical Review Letters* **78**, 674 (1997).
- [8] A. H. Boozer, Plasma equilibrium with rational magnetic surfaces, *The Physics of Fluids* **24**, 1999 (1981).
- [9] A. H. Boozer, Transport and isomorphic equilibria, *The Physics of Fluids* **26**, 496 (1983).
- [10] J. Nührenberg and R. Zille, Stable stellarators with medium β and aspect ratio, *Physics Letters A* **114**, 129 (1986).
- [11] F. S. B. Anderson, A. F. Almagri, D. T. Anderson, P. G. Matthews, J. N. Talmadge, and J. L. Shohet, The Helically Symmetric Experiment, (HSX) Goals, Design and Status, *Fusion Technology* **27**, 273 (1995).
- [12] M. C. Zarnstorff, L. A. Berry, A. Brooks, E. Fredrickson, G.-Y. Fu, S. Hirshman, S. Hudson, L.-P. Ku, E. Lazarus, D. Mikkelsen, D. Monticello, G. H. Neilson, N. Pomphrey, A. Reiman, D. Spong, D. Strickler, A. Boozer, W. A. Cooper, R. Goldston, R. Hatcher, M. Isaev, C. Kessel, J. Lewandowski, J. F. Lyon, P. Merkel, H. Mynick, B. E. Nelson, C. Nührenberg, M. Redi, W. Reiersen, P. Rutherford, R. Sanchez, J. Schmidt, and R. B. White, Physics of the compact advanced stellarator NCSX, *Plasma Physics and Controlled Fusion* **43**, A237 (2001).
- [13] H. Liu, A. Shimizu, Y. Xu, S. Okamura, S. Kinoshita, M. Isobe, Y. Li, G. Xiong, X. Wang, J. Huang, J. Cheng, H. Liu, X. Zhang, D. Yin, Y. Wang, T. Murase, S. Nakagawa, and C. Tang, Configuration characteristics of the Chinese First Quasi-axisymmetric Stellarator, *Nuclear Fusion* **61**, 016014 (2020).
- [14] T. Qian, M. Zarnstorff, D. Bishop, A. Chamblis, A. Dominguez, C. Pagano, D. Patch, and C. Zhu, Simpler optimized stellarators using permanent magnets, *Nuclear Fusion* **62**, 084001 (2022).
- [15] M. Landreman and E. Paul, Magnetic Fields with Precise Quasisymmetry for Plasma Confinement, *Physical Review Letters* **128**, 035001 (2022).
- [16] S. P. Hirshman and J. C. Whitson, Steepest-descent moment method for three-dimensional magnetohydrodynamic equilibria, *The Physics of Fluids* **26**, 3553 (1983).
- [17] S. Gori, W. Lotz, and J. Nührenberg, Theory of fusion plasmas, in *Proceedings of the Joint Varenna–Lausanne International Workshop 1996* (Editrice Compositori, Bologna, 1996) p. 335.
- [18] D. A. Spong, S. P. Hirshman, L. A. Berry, J. F. Lyon, R. H. Fowler, D. J. Strickler, M. J. Cole, B. N. Nelson, D. E. Williamson, A. S. Ware, D. Alban, R. Sánchez, G. Y. Fu, D. A. Monticello, W. H. Miner, and P. M. Valanju, Physics issues of compact drift optimized stellarators, *Nuclear Fusion* **41**, 711 (2001).
- [19] A. A. Subbotin, M. I. Mikhailov, V. D. Shafranov, M. Y. Isaev, C. Nührenberg, J. Nührenberg, R. Zille, V. V. Nemov, S. V. Kasilov, V. N. Kalyuzhnyj, and W. A. Cooper, Integrated physics optimization of a quasi-isodynamic stellarator with poloidally closed contours of the magnetic field strength, *Nuclear Fusion* **46**, 921 (2006).
- [20] A. G. Goodman, K. C. Mata, S. A. Henneberg, R. Jorge, M. Landreman, G. G. Plunk, H. M. Smith, R. J. J. Mackenbach, C. D. Beidler, and P. Helander, Constructing precisely quasi-isodynamic magnetic fields, *Journal of Plasma Physics* **89**, 905890504 (2023).
- [21] D. W. Dudt, A. G. Goodman, R. Conlin, D. Panici, and E. Kolemen, Magnetic fields with general omnigenity, *Journal of Plasma Physics* **90**, 905900120 (2024).
- [22] A. G. Goodman, P. Xanthopoulos, G. G. Plunk, H. Smith, C. Nührenberg, C. D. Beidler, S. A. Henneberg, G. Roberg-Clark, M. Drevlak, and P. Helander, Quasi-Isodynamic Stellarators with Low Turbulence as Fusion Reactor Candidates, *PRX Energy* **3**, 023010 (2024).
- [23] P. Helander, A. G. Goodman, C. D. Beidler, M. Kuczyński, and H. M. Smith, Optimised stellarators with a positive radial electric field (2024), arXiv:2405.07085.
- [24] G. G. Plunk, M. Landreman, and P. Helander, Direct construction of optimized stellarator shapes. Part 3. Omnigenity near the magnetic axis, *Journal of Plasma Physics* **85**, 905850602 (2019).
- [25] R. Jorge, G. G. Plunk, M. Drevlak, M. Landreman, J.-F. Lobsien, K. C. Mata, and P. Helander, A single-field-period quasi-isodynamic stellarator, *Journal of Plasma Physics* **88**, 175880504 (2022).
- [26] K. C. Mata, G. G. Plunk, and R. Jorge, Direct construction of stellarator-symmetric quasi-isodynamic magnetic configurations, *Journal of Plasma Physics* **88**, 905880503 (2022).
- [27] E. Rodriguez and G. G. Plunk, Higher order theory of quasi-isodynamicity near the magnetic axis of stellarators (2023), arXiv:2303.06038.
- [28] E. Sánchez, J. L. Velasco, I. Calvo, and S. Mulas, A quasi-isodynamic configuration with good confinement of fast ions at low plasma β , *Nuclear Fusion* **63**, 066037 (2023).
- [29] J. L. Velasco, I. Calvo, E. Sánchez, and F. I. Parra, Robust stellarator optimization via flat mirror magnetic fields, *Nuclear Fusion* **63**, 126038 (2023).
- [30] J. R. Cary and S. G. Shasharina, Omnigenity and quasi-helicity in helical plasma confinement systems, *Physics of Plasmas* **4**, 3323 (1997).
- [31] M. Landreman and P. J. Catto, Omnigenity as generalized quasisymmetry, *Physics of Plasmas* **19**, 056103 (2012).
- [32] S. Lazerson, J. Schmitt, C. Zhu, J. Breslau, and A. STELLOPT Developers, *Stellopt* (2020).
- [33] M. Landreman, B. Medasani, F. Wechsung, A. Giuliani, R. Jorge, and C. Zhu, SIMSOPT: A flexible framework

- for stellarator optimization, *Journal of Open Source Software* **6**, 3525 (2021).
- [34] D. W. Dudt, R. Conlin, D. Panici, and E. Kolemen, The DESC stellarator code suite Part 3: Quasi-symmetry optimization, *Journal of Plasma Physics* **89**, 955890201 (2023).
- [35] P. Virtanen, R. Gommers, T. E. Oliphant, M. Haberland, T. Reddy, D. Cournapeau, E. Burovski, P. Peterson, W. Weckesser, J. Bright, S. J. van der Walt, M. Brett, J. Wilson, K. J. Millman, N. Mayorov, A. R. J. Nelson, E. Jones, R. Kern, E. Larson, C. J. Carey, Í. Polat, Y. Feng, E. W. Moore, J. VanderPlas, D. Laxalde, J. Perktold, R. Cimrman, I. Henriksen, E. A. Quintero, C. R. Harris, A. M. Archibald, A. H. Ribeiro, F. Pedregosa, and P. van Mulbregt, *SciPy 1.0: Fundamental algorithms for scientific computing in Python*, *Nature Methods* **17**, 261 (2020).
- [36] S. R. Hudson, R. L. Dewar, G. Dennis, M. J. Hole, M. McGann, G. von Nessi, and S. Lazerson, Computation of multi-region relaxed magnetohydrodynamic equilibria, *Physics of Plasmas* **19**, 112502 (2012).
- [37] See Supplemental Material.
- [38] A. Dinklage, C. D. Beidler, P. Helander, G. Fuchert, H. Maaßberg, K. Rahbarnia, T. Sunn Pedersen, Y. Turkin, R. C. Wolf, A. Alonso, T. Andreeva, B. Blackwell, S. Bozhnikov, B. Buttenschön, A. Czarnecka, F. Effenberg, Y. Feng, J. Geiger, M. Hirsch, U. Höfel, M. Jakubowski, T. Klinger, J. Knauer, G. Kocsis, A. Krämer-Flecken, M. Kubkowska, A. Langenberg, H. P. Laqua, N. Marushchenko, A. Mollén, U. Neuner, H. Niemann, E. Pasch, N. Pablant, L. Rudischhauser, H. M. Smith, O. Schmitz, T. Stange, T. Szepesi, G. Weir, T. Windisch, G. A. Wurden, and D. Zhang, Magnetic configuration effects on the Wendelstein 7-X stellarator, *Nature Physics* **14**, 855 (2018).
- [39] V. V. Nemov, S. V. Kasilov, W. Kernbichler, and M. F. Heyn, Evaluation of $1/\nu$ neoclassical transport in stellarators, *Physics of Plasmas* **6**, 4622 (1999).
- [40] C. G. Albert, S. V. Kasilov, and W. Kernbichler, Symplectic integration with non-canonical quadrature for guiding-center orbits in magnetic confinement devices, *Journal of Computational Physics* **403**, 109065 (2020).
- [41] M. Yu. Isaev, M. I. Mikhailov, D. A. Monticello, H. E. Mynick, A. A. Subbotin, L. P. Ku, and A. H. Reiman, The pseudo-symmetric optimization of the National Compact Stellarator Experiment, *Physics of Plasmas* **6**, 3174 (1999).
- [42] M. Yokoyama, N. Nakajima, and M. Okamoto, Realization and classification of symmetric stellarator configurations through plasma boundary modulations, *Nuclear Fusion* **38**, 681 (1998).
- [43] A. A. Skovoroda, Comment on ‘Bootstrap current and neoclassical transport in quasi-isodynamic stellarators’, *Plasma Physics and Controlled Fusion* **53**, 038001 (2011).
- [44] J. W. Burby, R. S. MacKay, and S. Naik, Isodrastic Magnetic fields for suppressing transitions in guiding-centre motion, *Nonlinearity* **36**, 5884 (2023), arXiv:2211.13367 [physics].
- [45] J. L. Velasco, I. Calvo, F. J. Escoto, E. Sánchez, H. Thienpondt, and F. I. Parra, Piecewise Omnigenous Stellarators, *Physical Review Letters* **133**, 185101 (2024).
- [46] J. L. Velasco, E. Sánchez, and I. Calvo, Exploration of the parameter space of piecewise omnigenous stellarator magnetic fields (2024), arXiv:2412.14871 [physics].
- [47] H. E. Mynick, T. K. Chu, and A. H. Boozer, Class of Model Stellarator Fields with Enhanced Confinement, *Physical Review Letters* **48**, 322 (1982).
- [48] C. Zhu, S. R. Hudson, Y. Song, and Y. Wan, New method to design stellarator coils without the winding surface, *Nuclear Fusion* **58**, 016008 (2018).

Supplemental material for “Optimizing omnigenity like quasisymmetry for stellarators”

Hengqian Liu, Guodong Yu, Caoxiang Zhu, and Ge Zhuang

(Dated: February 13, 2025)

This document provides some numerical details and examines several physical properties, including Poincaré plots, rotational transform profiles, and \mathcal{J} distributions of the pwO configuration.

OPTIMIZATION SETTINGS AND FLUX SURFACE QUALITY

The optimization presented in this Letter was performed using SIMSOPT with VMEC serving as the MHD equilibrium solver. The degrees of freedom in the optimization process are the Fourier coefficients that describe the plasma boundary.

For the TO and HO cases, QA/QH were obtained first, starting with MPOL = 3, NTOR = 3, NS = 50, and a tolerance of FTOL = 10^{-11} . During the optimization process, MPOL and NTOR were incrementally increased until MPOL = 5 and NTOR = 5, while the highest Fourier mode describing the boundary shape was set to be MPOL - 2 and NTOR - 2. Once a satisfactory QA/QH configuration was obtained, the TO/HO optimization proceeded with a gradual increase in MPOL and NTOR up to MPOL = 12 and NTOR = 12, respectively, with the maximum Fourier mode of the boundary shape reaching 7. For the PO case, the optimization was initiated with MPOL = 3, NTOR = 3, NS = 50, and FTOL = 10^{-14} . MPOL and NTOR were progressively increased during the optimization until MPOL = 13 and NTOR = 13. The highest Fourier mode describing the boundary shape was incrementally increased from 1 to 7.

To ensure the accuracy of the final configuration, high-resolution VMEC runs were conducted with MPOL = 16, NTOR = 16 for TO, MPOL = 13, NTOR = 16 for HO, MPOL = 12, NTOR = 12 for PS & pwO, with NS = 201 and FTOL = 10^{-16} to ensure proper convergence. For the PO case, we used MPOL = 13, NTOR = 13, NS = 121 and FTOL = 10^{-16} to ensure convergence.

Magnetic islands induce substantial radial transport and can give rise to severe instabilities; thus, their presence should generally be minimized. The imposed constraint on the rotational transform serves to mitigate the occurrence of low-poloidal-mode-number rational surfaces. During the optimization process, the entire ι pro-

file was not explicitly controlled. Instead, the rotational transform was constrained either on a single flux surface or in terms of its average value. Consequently, it was necessary to examine the quality of the flux surfaces. To this end, we employed the SPEC code, as VMEC assumes the existence of nested flux surfaces. The last closed flux surface (LCFS) from VMEC was imported into SPEC, with the main simulation parameters set to NVOL = 1 and Lrad = 8. The values of MPOL and NTOR were maintained consistent with those in VMEC. The Beltrami equation was solved linearly using the GMRES solver iterating until the precision reached below 10^{-14} . Fig. 1 shows the SPEC results together with the rotational transform profiles. All five configurations have *no* magnetic islands or chaos inside the LCFS. The final ι profiles are also plotted in Fig. 1(f).

J DISTRIBUTIONS IN THE PWO CONFIGURATION

Here, we examine the \mathcal{J} distribution of the pwO configuration to check if the pwO characteristics are satisfied. The calculations were done on the outermost magnetic surface. 50 magnetic field lines were selected uniformly over the field line label $\alpha \in [0, 2\pi)$, and each field line was traced for 100 periods. The bounce points for different field strengths $B^* = (1 - t)B_{min} + tB_{max}$ were calculated. 200 values for the relative strength t uniformly distributed in $[0.05, 0.95]$ were used to scan B^* . Figure 2 shows the results. Unlike omnigenous configurations where \mathcal{J} has only a single principal value, pwO can have either a single value (low field) or three discrete values for \mathcal{J} (high field), consistent with the fact that pwO has the same minimum for B while having different values for B_{max} . However, the three discrete values of \mathcal{J} in the high field region, $\mathcal{J}^I, \mathcal{J}^{II}, \mathcal{J}^{III}$, satisfy the relationship of $\mathcal{J}^I + \mathcal{J}^{II} - \mathcal{J}^{III} = 0$, which is exactly the characteristic of the piecewise omnigenity concept. This condition ensures good particle confinement. The \mathcal{J} distribution also confirms that the pwO configuration in the Letter is a combination of omnigenity and piecewise omnigenity.

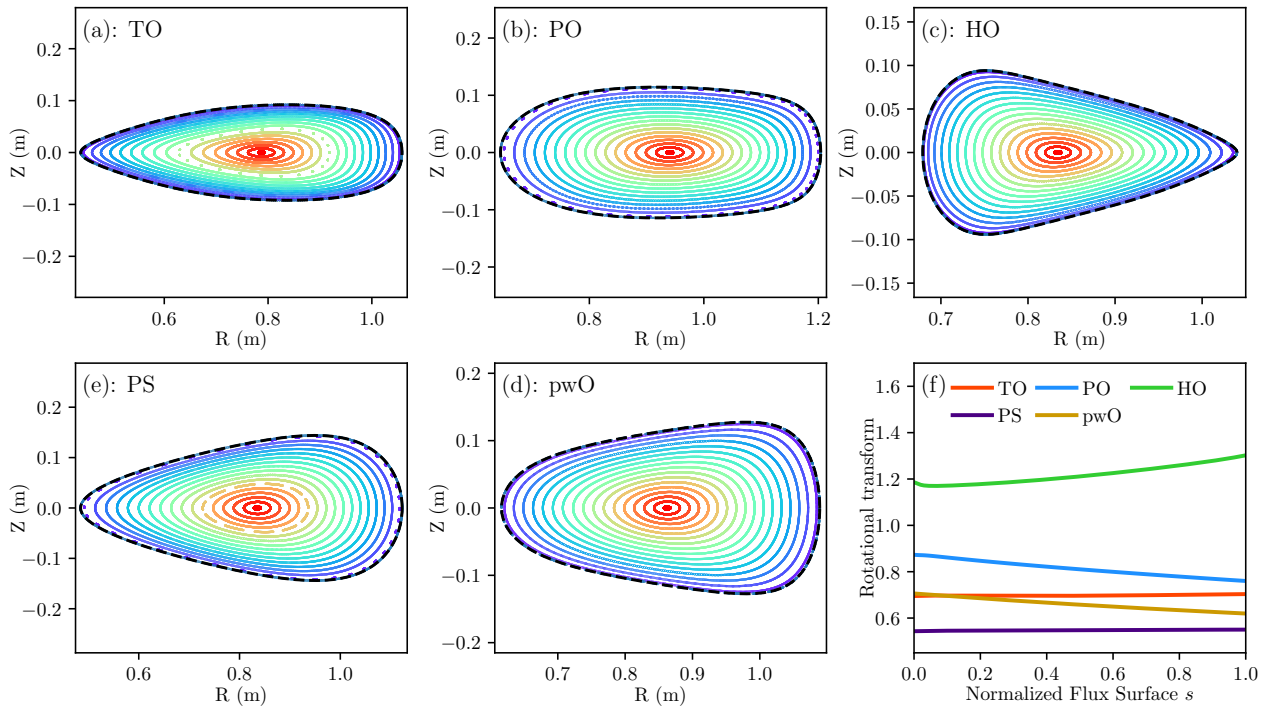


FIG. 1: (a)~(e): Poincaré plots from SPEC at toroidal angle $\phi = \pi/n_{fp}$ for TO, PO, HO, PS, and pwO. (Colors are only for better visualization.) Black dashed lines are the VMEC boundaries. (f): Rotational transform profiles for the five configurations.

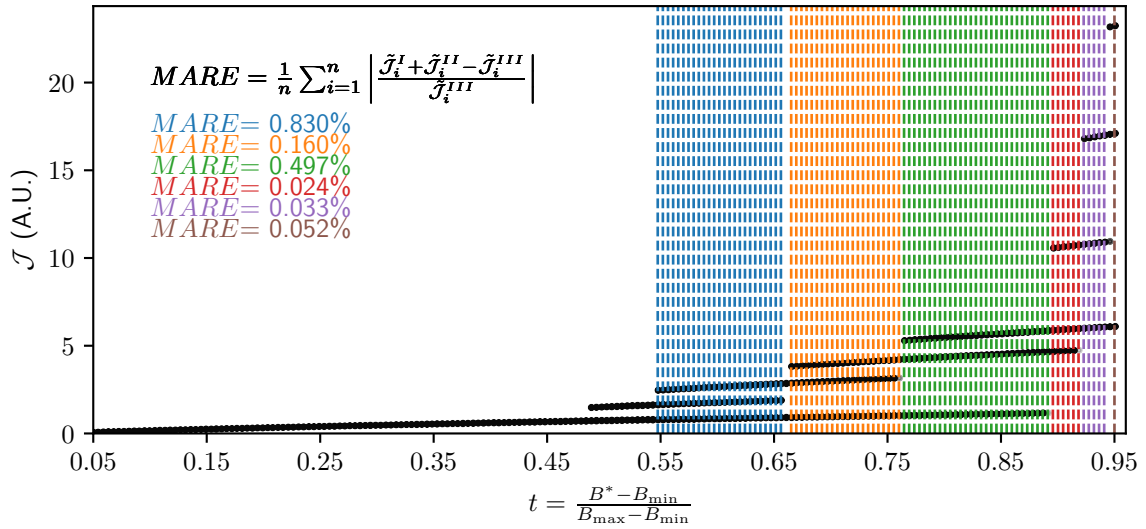


FIG. 2: \mathcal{J} distribution on the outmost magnetic surface of the pwO configuration. Each colored region represents an area where \mathcal{J} has three distinct principal values and the condition $\mathcal{J}^I + \mathcal{J}^{II} - \mathcal{J}^{III} = 0$ is satisfied.